Nabaa M. Abdul Rahim
Mohammed A. Kadhim
Fadhil K. Fuliful

Department of Physics,
College of Science,
University of Kerbala,
Karbala, IRAQ

Flame Coating of Stainless Steel 316 with Calcium Phosphate for Biocompatible Uses

The aim of the present work is to prepare a biocompatible layer utilizing flame coating technology, and the biocompatibility of the simulated body fluids (SBF) is examined. Separately prepared calcium and phosphate solutions (0.2 M) were combined at various Ca/P molar ratios (1.4, 1.5, 1.65, 1.8, and 1.9), and a nozzle-thrown flame was used to spray the mixture at a pressure of 4 bar via the control valve. Three centimeters away from the flame orifice, the droplets contact the flame and deposit on the stainless steel 316 surfaces. Analytical data were obtained by the use of Fourier-transform infrared spectroscopy (FTIR) and X-ray diffraction (XRD). The results show that when the Ca/P ratio rose to 1.65, the peak intensity increased, and as the ratio increased, it declined. A greater degree of crystallization and a development in crystal size are also indicated by the width of the peaks decreasing in the same proportion.

***Keywords*:** Medical implants; Flame coating; Calcium phosphate; Biocompatibility
Received: 25 May 2024; **Revised:** 07 October 2024; **Accepted:** 14 October 2024

1. Introduction

Flame coating, which is used for medical implants, melts the spray coating material using the heat produced by the combustion of a fuel gas, often acetylene, with oxygen. Biomaterials can be categorized as natural or artificial, and they fall under the ceramics, polymers, and composite materials categories. Medical implants are commonly utilized with biomaterials, which are thought to be the most common technology. It was employed to safely and acceptably replace a body part [1-3]. Biocompatible refers to a broad class of biomaterials used when introducing any material into the body without triggering an immune reaction [4,5]. The biological material is analyzed using x-ray diffraction (XRD) as well as Fourier-transform infrared (FTIR) spectroscopy. Orthopedic implants serve a variety of purposes, including joint and fracture stabilization, deformity correction, and many more. It helps to reduce discomfort and gives the bone the mechanical stability needed to preserve bone function. Bone repair and implants are closely related [6]. One of the earliest bio-metallic materials used in the production of orthopedic implants was stainless steel. When it first hit the market in 1920, its strong corrosion resistance made it stand out from other alloys. The 316 stainless steel is the most widely used form of stainless steel and has been effectively utilized for many years. Because it was readily available and simple to handle, it was regarded as a feasible implant [7,8]. Minerals are coated with biocompatible materials, and because of its biocompatible coating that resembles bone and is biologically active, hydroxyapatite can create a strong link between the implant and the bone. The essential activity of hydroxyapatite, which is thought to be a crucial factor in implant stability and lifetime in the human body, has been examined [9-11].

Several materials can be coated with calcium phosphate to increase their bioactivity. Depending on its unique bioactive qualities and bone regeneration efficacy [12]. Researchers discovered a variety of alloys to test for biocompatibility hydroxyapatite-coated metal. Titanium coated with first-grade HA performed the best when it came to possible implants [13-15].

In this work, a system for flame coating is designed and constructed. A calcium phosphate layer that is biocompatible is produced by flame coating on stainless steel 316 substrates, and the resulting layer is examined for potential application as human-compatible medical implants. In addition, a number of variables (such as the ratio of the components and the separation between the flame source and the bases) influenced the properties of the deposited films, and the characteristics of these films were studied.

2. Experimental Part

The materials utilized in this work are ammonium hydroxide solution (NH_4OH) from Alpha Aesar Chemical Co., di-ammonium hydrogen phosphate $(NH_4)2HPO_4$ (>99% purity) from Merck Co., and calcium nitrate ($Ca(NO_3)_2{:}4H_2O$) (98% purity) from Shanxi Leixin Chemical Co. The 316 stainless steel substrates provide a smooth surface, good resistance to corrosion, great formability, and high fabrication ease. Steel's physical qualities include heat resistance and high temperature resistance, while its chemical and electrochemical corrosion resistance is the finest.

A straightforward flame coating system is created and constructed in this study. Substrates made of stainless steel 316 are sliced, rinsed with water, and treated with alcohol. Separately produced, the 0.2 M calcium and phosphate solutions are combined at various Ca/P molar ratios (1.4, 1.5, 1.65, 1.8, and 1.9),

and a nozzle-thrown flame is used to spray the mixture at a pressure of 5 bar via the control valve. As seen in Fig. (1), the droplets interact with the flame and land on the stainless steel substrates three centimeters from the flame opening. Table (1) displays the molar and weight ratios for each of the five samples.

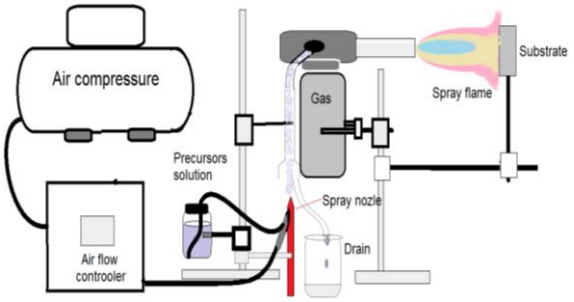

Fig. (1) Scheme of the flame coating setup

Table (1) Molar and weight ratios for the samples

Ca/P	Molar Ratio (x)		Weight in 20 ml D.W (g)	
	$Ca(NO_3)_2{:}4H_2O$	$(NH_4)_2HPO_4$	$Ca(NO_3)_2{:}4H_2O$	$(NH_4)_2HPO_4$
1.4	0.5833	0.4167	1.3773	0.5503
1.5	0.6000	0.4000	1.4166	0.5282
1.65	0.6226	0.3774	1.4701	0.4983
1.8	0.6429	0.3571	1.5178	0.4716
1.9	0.6552	0.3448	1.5469	0.4554

As seen in Fig. (2), the best deposited film occurs at a distance of 3 cm; at 2 cm, no film forms. The deposited distances are 2, 3, 4, 5, and 6 cm from the flame opening.

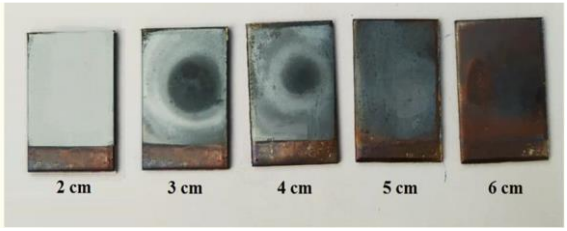

Fig. (2) Image of the samples prepared in this work

3. Results and Discussion

On a stainless steel substrate, the biocompatible layers made via flame coating were applied in various calcium phosphate ratios. A Shimadzu XRD 6000 X-ray diffractometer was used to characterize the films with a Cu (Kα) radiation source (wavelength of 1.5405Å) and scanning speed of 5.00 deg/min. The FTIR analysis of the layer's chemical band was conducted using a ThermoScientific Nicolet N10 FTIR spectrometer.

Calcium and phosphate solutions that were prepared separately and at different molar ratios of Ca/P (1.4, 1.5, 1.65, 1.8, and 1.9) were mixed together. The deposited layers were formed on the substrate 3 cm away from the flame entrance. The XRD patterns of the deposited layers are shown in Fig. (3). Each sample showed a polycrystalline tetragonal structure of calcium diphosphate in beta phase that was consistent with the standard JCPDS card 96-100-1557. A number of peaks that corresponded to the lattice planes (114), (211), (124), (215), (029), (02 11), (309), (236), (11 14), and (30 12) emerged at diffraction angles 2θ = 24.2633°, 30.2369°, 33.2718°, 35.5600°, 43.1473°, 49.4099°, 53.5046°, 54.1068°, 57.0213°, and 62.5853°. due to variations in lattice strain or crystalline size. This causes slight changes in the peak positions caused by lattice strain [16].

The direction of (215) was the preferred orientation; also, the peak intensity increased with a 1.65 Ca/P ratio and decreased with an increase in ratio due to the decreasing film thicknesses. On the other hand, the widest point and maximum expansion in crystallite size are reached when the ratio between the peaks declines.

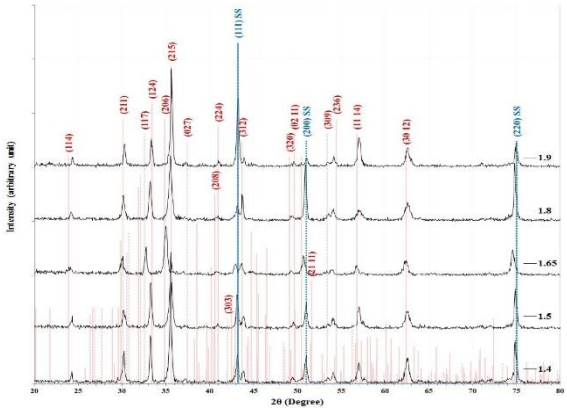

Fig. (3) XRD patterns of calcium phosphate layers deposited with different Ca/P ratios

Using the two peaks of directions (215) and (3012), the lattice constants (a) and (c) for the calcium phosphate tetragonal structure are computed using the following equations [17]

$$\frac{1}{h^2_{khl}}=\frac{h^2+k^2}{a^2}+\frac{l^2}{c^2} \quad (1)$$

Then by substituting $\frac{1}{h^2_{khl}}=\frac{4sin^2\theta_{hkl}}{n^2\lambda^2}$ from the Bragg's law can written as

$$sin^2\theta_{hkl} = A(h^2+k^2)+Cl^2 \quad (2)$$

where $A = \lambda^2/4a^2$, $C = \lambda^2/4c^2$

$$sin^2(35.60) = 5A + 25C \quad (3a)$$

$$sin^2(62.58) = 9A + 144C \quad (3b)$$

Solving the two equations (3a,b) for the two selected lines can measure the lattice constants as shown in table (2).

Table (2) Lattice constants for calcium phosphate layers deposited at different Ca/P ratios

Ca/P	a (Å)	c (Å)
1.4	6.6425	24.0578
1.5	6.6309	24.0422
1.65	6.6155	24.0229
1.8	6.6653	24.0258
1.9	6.6745	24.2458

The identification of bonds depends on the preparation conditions; however, as can be observed for different Ca/P ratios in Fig. (4), the bond values are very constant throughout all samples, even with these fluctuations. There are two bands identified in the phosphate group; the first has three peaks (1082.69, 1019.29, and 903.03 cm^{-1}), while the second has (579.65, 539.49, and 471.86 cm^{-1}) bands. These bands indicate the calcium-phosphate structure [18]. The analyses confirmed that the samples included carbonate ions, as evidenced by bands that appeared at 1412.42, 1082.69, and 805.81 cm^{-1}. The use of combustible gas during the deposition process causes these bands. Moreover, OH bands centered at 3400, 1640.69, and 645.17 cm^{-1}, which are ascribed to the adsorbed water molecules, were observed on the sample surface.

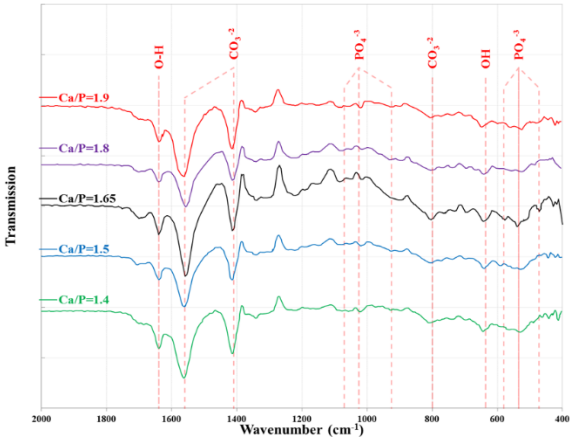

Fig. (4) FTIR spectra of calcium phosphate layers deposited with different Ca/P ratios

Table (3) Vibrational bands for the prepared samples at various Ca/P ratios

Band type	Ca/P ratio				
	1.4	1.5	1.65	1.8	1.9
O-H	1638.57	1640.69	1640.69	1640.69	1640.69
CO_3^{-2}	1562.48	1564.60	1558.26	1558.26	1566.71
	1414.53	1416.64	1412.42	1414.53	1414.53
PO_4^{-3}	1076.35	-	1082.69	1074.24	1082.69
	1021.40	1021.40	1023.29	1021.40	1021.40
	924.17	928.40	935.03	-	924.17
CO_3^{-2}	810.04	805.81	805.81	803.69	805.81
OH	647.29	643.07	645.17	643.06	649.40
PO_4^{-3}	-	592.34	579.65	-	560.63
	533.16	526.82	539.49	524.70	524.70
	463.41	-	471.86	484.54	476.09

All samples appear to have a high carbonate content based on the high intensity of the carbonate bands in comparison to the phosphate bands. The phosphate peaks of the Ca/P = 1.65 ratio are the best when compared to other samples of the ratios (1.4, 1.5, 1.8, and 1.9). The maximum levels of phosphate were observed in the two center peaks at a ratio of 1.65 and the behavior of bond energy and peak intensity is comparable. In bone tissue, hydroxyapatite is present together with other trace minerals. It contains organic components that form the matrix of bone tissues as well as collagen, which is detectable in the FTIR spectrum. The infrared spectra bands for each of the five samples at various Ca/P ratios are displayed in table (3) [18]. Table (3) shows the vibrational bands of calcium phosphate layers deposited at different Ca/P ratios according to the FTIR results.

The simulated body fluid (SBF) method was employed to assess the deposited layers' biocompatibility. The elements listed in table (4) make up the SBF. To track the development of the hydroxyapatite layer on the substrates, the pH of the SBF liquid is measured during the immersion period of 21 days and controlled at 7.4 pH and 36.5 °C. It has been common practice to utilize a SBF with ion concentrations roughly equivalent to those of human blood plasma for the creation of bone-like apatite on a variety of substrates and for the in vitro evaluation of the bioactivity of artificial materials. However, blood plasma's ion concentrations and those of a conventional SBF are not exactly similar [20].

Table (4) SBF components [21]

Reagents	g/L
NaCl	8.3
$NaHCO_3$	0.35
KCl	0.22
$K_2HP_4.3H_2O$	0.23
$MgCl_2.6H_2O$	0.31
$CaCl_2$	0.29
Na_2SO_4	0.07

4. Conclusion

One easy and inexpensive method of creating the hydroxyapatite layers is by flame coating. Stainless steel 316 substrates are suitable for deposition processes. The SBF method as an in vitro predictor of a material's propensity to form bone bonds. The XRD test produced distinct calcium and phosphorus ratios, which indicated the biocompatibility of the material. Particularly the sample created with a ratio of 1.65, all samples displayed polycrystalline dicalcium phosphate for the first coating and extra peaks corresponding to the hydroxyapatite phase. Therefore this sample could be used in implants to speed up the growth of bone.

References

[1] K. Tappa and U. Jammalamadaka, "Novel biomaterials used in medical 3D printing techniques", *J. Func. Biomater.*, 9(1) (2018) 17.

[2] F.D. Al-Shalawi et al., "Biomaterials as Implants in the Orthopedic Field for Regenerative Medicine: Metal versus Synthetic Polymers", *Polymers*, 15(12), (2023) 2601.

[3] A. Carnicer-Lombarte et al., "Foreign Body Reaction to Implanted Biomaterials and Its Impact in Nerve Neuroprosthetics", *Front. Bioeng. Biotechnol*., 9 (2021) 622524.

[4] L. Kämmerling et al., "Mitigating the foreign body response through 'immune-instructive' biomaterials", *J. Immunol. Regener. Med.*, 12 (2021) 100040.
[5] A.M. Elgebali, E.S. Sami and B.A. Moharram, "Effects of Annealing and Substrate Temperatures on Dielectric Properties of CuInGaS2 Structures Prepared by Quenching-Assisted Vacuum Coating Technique", *Iraqi J. Mater.*, 3(3) (2024) 1-6.
[6] Q. Hong and B. Nie, "Special Issue: Multifunctional Coatings in Orthopedic Implants", *Coatings*, 12 (2022) 967.
[7] M.Z. Ibrahim et al., "Biomedical materials and techniques to improve the tribological, mechanical and biomedical properties of orthopedic implants", *J. Alloys Comp.*, 714 (2017) 636–667.
[8] K. Szwajka, J. Zielińska-Szwajka, and T. Trzepieciński, "Improving the Surface Integrity of 316L Steel in the Context of Bioimplant Applications", *Materials (Basel)*, 16(9) (2023) 3460.
[9] D. Govindaraj and M. Rajan, "Coating of Bio-mimetic Minerals-Substituted Hydroxyapatite on Surgical Grade Stainless Steel 316L by Electrophoretic Deposition for Hard tissue Applications", *IOP Conf. Series: Mater. Sci. Eng.*, 314 (2018) 012029.
[10] K.A. Kravanja and M. Finšgar, "A review of techniques for the application of bioactive coatings on metal-based implants to achieve controlled release of active ingredients", *Mater. Design*, 217 (2022) 110653.
[11] A. Bandyopadhyay et al., "Improving biocompatibility for next generation of metallic implants", *Prog. Mater. Sci.*, 133 (2023) 101053.
[12] J. Jeong et al., "Bioactive calcium phosphate materials and applications in bone regeneration", *Biomater. Res.*, 23(4) (2019).
[13] M. Furko et al., "Corrosion and biocompatibility examination of multi-element modified calcium phosphate bioceramic layers", *Mater. Sci. Eng. C*, 95 (2019) 381–388.
[14] A. Naderi et al., "Improved Biocompatible, Flexible Mesh Composites for Implant Applications via Hydroxyapatite Coating with Potential for 3-Dimensional Extracellular Matrix Network and Bone Regeneration", *ACS Appl. Mater. Interfaces*, 13(23) (2021) 26824-26840.
[15] G. Jodhani and P.I. Gouma, "Flame spray pyrolysis processing to produce metastable phases of metal oxides", *JOJ Mater. Sci.*, 1 (2017) 1–5.
[16] E.A. Ofudje et al., "Bioactivity properties of hydroxyapatite/clay nanocomposites", *Sci. Rep.*, 13 (2023) 19896.
[17] N. Saowadee, K. Agersted and J.R. Bowen, "Lattice constant measurement from electron backscatter diffraction patterns", *J. Microscopy*, 266(2) (2018) 200-210.
[18] V.K. Singh et al., "Application of WDXRF and FT-IR for Human Tooth Analysis", *Spectroscopy*, 34(12) (2019) 23-32.
[19] M. Maqbool et al., "Synthesis, Characterization, Antibacterial Properties, and In Vitro Studies of Selenium and Strontium Co-Substituted Hydroxyapatite", *Int. J. Mol. Sci.*, 22(8) (2021) 4246.
[20] A. Oyane et al., "Preparation and Assessment of Revised Simulated Body Fluids", *J. Biomed. Mater. Res. A*, 65(2) (2003) 188-95.
[21] B.R. Gligorijević and M.N. Vilotijević, "Simulated Body Fluids Prepared with Natural Buffers and System for Active pH Regulation" *Iran. J. Chem. Chem. Eng.*, 41(9) (2022) 2918-2935.

